The measurement of object distance for projected virtual objects using a scanning pentaprism and digital alignment telescope

Kevin Sweeney[a], David A. Imrie[a]
[a]Optikos Corporation, 107 Audubon Road, Bldg. 3, Wakefield, MA 01880

ABSTRACT

A standard method for assessing collimation involves sampling a series of sub-apertures across the collimating optic and evaluating the local wavefront slope at each position. In practice, this is done by employing a sliding pentaprism to scan the smaller pupil of an alignment telescope across the collimator pupil. Variation in angle of incidence, recorded as image translation in the telescope, indicates collimation error.

We have increased the utility of this technique by automating the scanning motion, image collection, and tracking of the observed centroid at a sub-pixel level. Automating the measurement process ensures accurate and repeatable results by eliminating reliance on operator judgments of image quality and reticle positions. Furthermore, automation advances the application into the precise measurement of finite conjugate distances. An instrument based on these principles is capable of measuring the apparent distance of a virtual object, making the approach ideal for setting long conjugates in target projectors.

An analysis based in geometrical optics is presented which accounts for the variable standoff distance of the sampling aperture from the telescope objective. This analysis parameterizes the scanning pentaprism technique, allowing exploration of how the telescope focal length, scan length, and nominal standoff distance affect performance factors such as sensitivity to telescope focus error.

Measured data collected from a portable instrument based on the scanning pentaprism technique is included. The data demonstrates measurement of various conjugate distances ranging from infinity to 1 meter. When setting collimation for a 150mm f/10 off-axis paraboloidal mirror, the instrument enables us to routinely set the projected object to distances greater than 7.5km, corresponding with less than 2/3 λ residual power. A robust mechanical architecture allows the instrument to be hand-carried for characterization of large collimators and target projectors mounted at their point of use.

Keywords: Metrology, collimation, conjugate, wavefront, focus, alignment, portable, test

1. BACKGROUND

Testing the performance of an imaging system requires presenting an object of which an image will be formed in a conjugate plane. Because the optical transfer function of any imager is dependent on the specific conjugate plane at which it is used, presenting an object at a distance consistent with the intended application is critical to conducting a meaningful test. For the same reason, the spectrum of light transmitted, reflected, or emitted by the object should also match the application. This test beam must fill the entrance pupil of the imager-under-test, which can be considerably large for long focal length systems. A variety of possible object distances and spectra imposes the need for a versatile test beam verification instrument. To support testing of large imaging systems, the instrument should be portable so that it can be brought to the test area for in situ characterization.

Test methods may also require specific object geometries such as pinholes, crosshairs, crossedges, or more complicated patterns. Accommodating extended objects precludes interferometric and Shack-Hartmann wavefront sensing techniques which rely on pupil imaging. Instead, the instrument sensor should resolve an image of the object itself for the analysis.

An apparatus that enables testing of large aperture optics without needing larger reference optics is first described by Wetthauer and Brodhun [1]. It triangulates the precise location of the focus by translating a small collimated beam across

the pupil of the lens-under-test while the range of spot translation is observed at two screens on either side of the approximate focal plane. The key innovation of this technique is fixing the collimator perpendicular to the axis of the lens-under-test and moving only a pentaprism for beam scanning. The pentaprism property of constant deflection angle drastically reduces the straightness required of the linear guideway.

This scanning pentaprism approach finds regular but not widespread use in testing astronomical telescopes [2]. The pentaprism test is incorporated to detect spherical aberration which can result from using an erroneous null lens for interferometric feedback during surface figuring [3, 4]. Often the direction of light travel is reversed: The light source is moved to the focal plane of the telescope-under-test, and is replaced in what was previously the collimator by an eyepiece to form an alignment telescope. Alternatively an image sensor can record the spot translation, increasing measurement speed and allowing for automation.

Another class of optics requiring large aperture testing is grazing incidence mirrors used in synchrotron radiation beam lines. It is advantageous to test these mirrors in situ so that their form is measured under heat loads sustained during operation [5]. A proposed surface profiler [6] leverages the scanning pentaprism approach, but using a pencil beam interferometer [7] to both project and receive light through the pentaprism. The interferometer can be replaced with an autocollimating telescope [8] to return to an imaging modality. This application illustrates the potential of a scanning pentaprism architecture for portable and inexpensive instrumentation.

The light source may also be integrated into the lens-under-test, forming a target projector for performance characterization of imagers. Achieving low uncertainty in the conjugate plane at which the imager is tested requires the target projector to have a longer focal length than the imager, such that focus errors in the target projector are reduced at the imager conjugate plane via longitudinal magnification. The scanning pentaprism method is identified in the international standard for measurement of the optical transfer function [9] as an effective means of minimizing the target projector contribution to focus error.

Mohammadi, Lee, and Jennewein [10] demonstrate characterization of a collimating target projector using commercially available components. A collimated beam comprises parallel rays which will nominally travel through the alignment telescope along the same path. In this way, collimation represents a limiting case where the scanning pentaprism test becomes a null measurement. For the general case of beams converging to or diverging from finite object distances, the ray paths travel through the apparatus in a dynamic way. Careful consideration of the optical layout of the instrument and how rays propagate through it is necessary to avoid systematic error.

2. ANALYSIS

A scanning pentaprism measurement of object distance is shown schematically in Figure 1. The object distance t is the total distance along the telescope line of sight from the telescope objective lens to the object. In our diagrams, we will draw the object and images of the object as crossedge symbols, so that it is clear where these conjugate points lie. Although the schematic is drawn for the case of a real object located a finite distance in front of the apparatus, measuring virtual or real images of objects projected through relay optics is also possible. This means the method can measure collimated objects (where $t \to \infty$), and beams that are converging to real images (where $t < 0$).

An alignment telescope objective lens with positive focal length f collects rays sampled from the test beam and relays them onto an image sensor. Here we assume that the image sensor lies in the focal plane of the objective lens. In this positive and finite object distance scenario, an image of the object would form behind the image sensor if the rays were not absorbed by the sensor pixels.

A pentaprism located a distance s in front of the objective lens deviates the beam produced by the object 90° from its initial direction of travel. The pentaprism can translate a distance $|2x|$ along the telescope line of sight, and across the object beam, centered on the nominal location defined by s. At each position x along this travel range, a ray is sampled from the object beam and relayed through the telescope objective lens. The point of intersection c is recorded by the image sensor, and the corresponding scan position x is recorded by the motion control system. The goal of the measurement is to process the function $c(x)$, which is proportional to $\theta(x)$, to derive the object distance t-s. We will refer to the functions $c(x)$ and $\theta(x)$ interchangeably as the ray fan, since this function is in fact the commonly utilized transverse ray aberration plot, colloquially referred to as the ray fan, of the beam.

As a convention, we will assume that the entire telescope and scanning pentaprism apparatus is aligned such that the central ray is colinear with the deviated line of sight of the alignment telescope when the pentaprism is at its center of travel position x=0. Positive x displacement from this position is in the direction moving away from the objective lens.

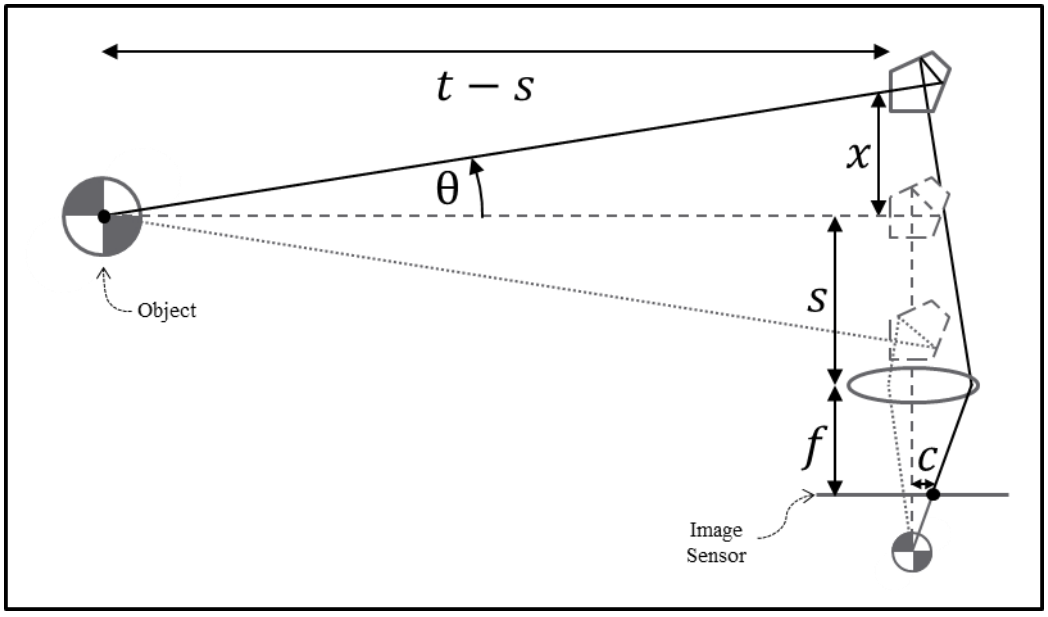

Figure 1. The scanning pentaprism layout. All distances are positive as drawn.

The asymmetric variation of ray paths through the objective lens in Figure 1 reveals a source of nonlinearity in the relationship between measured ray fan and object distance. This nonlinearity can become significant for short object distances, especially as object distance becomes comparable in magnitude to the focal length of the telescope or the nominal pentaprism distance s. Both of these relationships arise from the scanning pentaprism defining the aperture stop of the imaging system, with the stop changing location as the pentaprism samples rays across the beam. Because the stop is at a fold in the optical path, the motion influences the measurement in two distinct ways that are individually apparent when considering stop motion firstly relative to the object, and secondly from the perspective of the telescope.

The aperture stop defines the optical axis of the measurement apparatus. As the stop translates laterally to sample various rays in the beam, the optical axis becomes offset from the object. Or in reference frame of the optical axis, the object apparently translates off-axis. This means that the real image will also translate off-axis at a rate defined by the transverse magnification of the telescope imaging system, which is dependent on object distance which of course is not known at the time of measurement.

From the perspective of the telescope objective lens, the aperture stop translates forward and backward along the optical axis. This changes the object distance to the objective lens, and consequently the magnification of the image, by an amount that varies throughout a measurement. This motion also varies the distance between the aperture stop and the objective lens, leading to the asymmetry of ray paths through the lens even when measuring a symmetrical beam.

A geometrical optics analysis can parametrize the effects of this stop motion in any measurement, so that it may be accounted for in the computation of object distance. To aid this analysis, Figure 2 unfolds the optical schematic from Figure 1 and labels several important points along a chief ray collected by the system. The points are referenced to an origin at the center of the objective lens. The subtraction of the x scan position from the horizontal coordinates of the object and scanning pentaprism aperture as well as the inclusion of x in the vertical off-axis distance of the object account for all of the stop shift effects discussed above. We have also added a defocus factor Δf for the image sensor, which can be assumed to be zero for a sensor that is well focused for an infinite conjugate.

Chief Ray Analysis

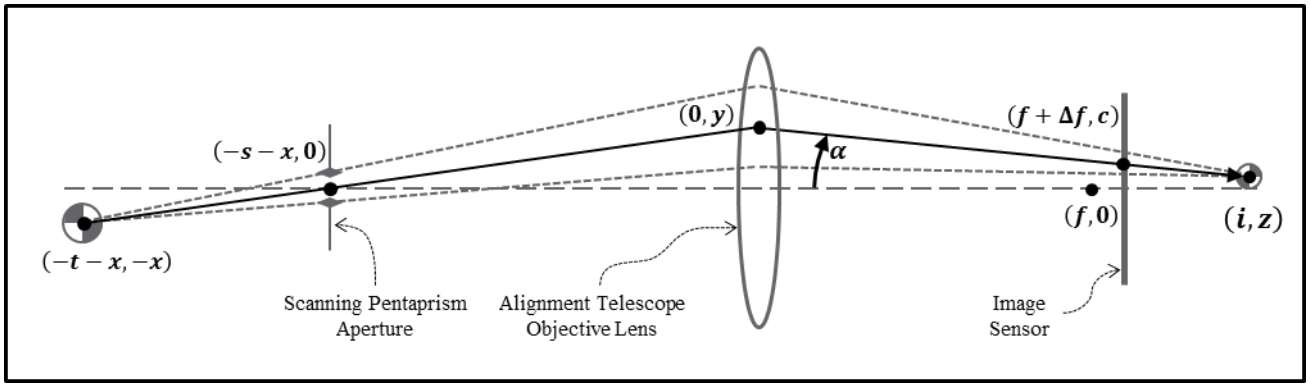

Figure 2. Unfolded scanning pentaprism chief ray trace with important points denoted in a Cartesian coordinate system with origin (0,0) at the center of the telescope objective lens. The additional ray path length within the pentaprism compared to the simpler reflection case of a 45° fold mirror is assumed to be negligible.

On the object side of the objective lens, the chief ray forms the hypotenuse of two similar triangles spanning the distance from the object to the scanning pentaprism aperture, and from the object to the lens. Setting the ratios of the bases of these triangles equal to each other leads to Equation 1 for the height of the chief ray when it intersects the objective lens.

$$y = \frac{x(t+x)}{t-s} - x$$

Equation 1. Height of the intersection of the chief ray with the alignment telescope objective lens.

Next we need an equation for the height of the image, so that it can be used in combination with the height of the lens intersection to triangulate the height of the sensor intersection. To do this, we will utilize the paraxial optics relationships for image location (Equation 2) and transverse magnification (Equation 3).

$$\frac{1}{i} = \frac{1}{f} + \frac{1}{-t-x}$$

Equation 2. Gaussian form of the Lensmaker's Equation for a thin alignment telescope objective lens.

$$m = \frac{i}{-t-x} = \frac{z}{-x}$$

Equation 3. Transverse magnification of the image.

Combining these relationships yields Equation 4 for the height of the chief ray in the conjugate plane of the alignment telescope objective lens.

$$z = \frac{x}{\frac{(t+x)}{f} - 1}$$

Equation 4. Height of the image for a thin alignment telescope objective lens.

From the heights of the chief ray at the lens and conjugate planes and the axial distance between these two planes we can calculate the chief ray angle in image space using Equation 5.

$$\tan \alpha = \frac{z - y}{i}$$

Equation 5. Chief ray angle in image space for a thin alignment telescope lens.

The above equations are combined in Equation 6 to calculate the height of the chief ray on the image sensor.

$$c = z - (i - f - \Delta f) \tan \alpha$$

Equation 6. Height of the chief ray in the image sensor plane for a thin alignment telescope lens.

The behavior of the chief ray is now parameterized in terms of values that are known by design (*s* and *f*), monitored during operation (*x* and *c*), and one unknown value that we intend to determine (*t*). Given a measured ray fan *c*(*x*), an iterative procedure can be used to find the value of *t* which matches the slope of Equation 6 to the slope of the measured ray fan. Table 1 describes the procedure which was used to calculate object distance in the Results section.

Step	**Iteration Step**	**Description**
1		Compute the slope of the measured ray fan.
2		Compute initial estimate of object distance *t* as the ratio *f / slope*.
3	a	Using the current estimate for object distance, compute the theoretical ray fan according to Equation 6.
	b	Calculate the slope of this theoretical ray fan.
	c	Calculate the ratio of theoretical slope to measured slope.
	d	Multiply current estimate for object distance by this ratio to establish a new estimate.
	e	Return to 3a and iterate until current estimate for object distance has converged.
4		Subtract *s* from the final estimate of *t* to report object distance from the plane of the scanning pentaprism aperture.

Table 1. Procedure for calculating object distance from a measured ray fan.

The sensitivity of ray fan slope to component and alignment uncertainties may also be explored using Equation 6. For instance, varying the defocus factor simulates focus error between the image sensor and objective lens. Figure 3 demonstrates this for several nominal pentaprism aperture spacings. The configuration s=1f minimizes sensitivity to defocus, as the scanning aperture travel is centered about the telecentric condition. These sensitivity factors are independent of object distance and scan range.

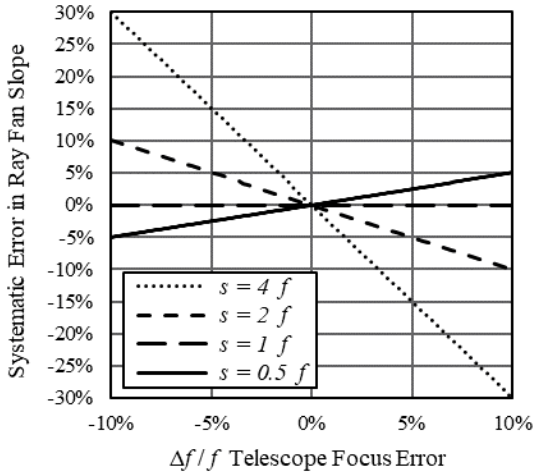

Figure 3. Sensitivity of ray fan slope to telescope focus error for various nominal pentaprism aperture spacings.

Marginal Ray Analysis

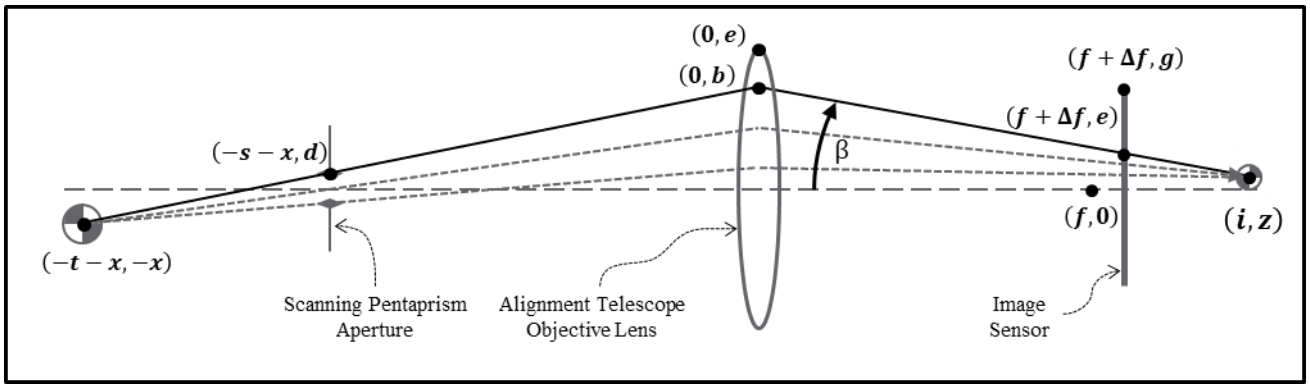

Figure 4. Marginal ray path through unfolded scanning pentaprism apparatus.

Considering the marginal ray defined by the scanning pentaprism aperture half width d (Figure 4) in the same manner as the chief ray analysis above leads to the similar set of equations Equation 7 through Equation 9.

$$b = \frac{(x+d)(t+x)}{t-s} - x$$

Equation 7. Height of the marginal ray at the point of intersection with the alignment telescope objective lens.

$$\tan\beta = \frac{z-b}{i}$$

Equation 8. Marginal ray angle in image space.

$$e = z - (i - f - \Delta f)\tan\beta$$

Equation 9. Height of the marginal ray intersection with the image sensor.

To avoid vignetting at the telescope objective lens, *b* must always be less than the lens semi-diameter *e*. Setting up this inequality using Equation 7 and solving the resulting quadratic equation in *x* leads to Equation 10 for the maximum scan length achievable with zero vignetting at the lens. Given the design parameters *d*, *e*, and *s*, and a use case measuring a certain distance *t*, one can use this equation to ensure that the scanning pentaprism is able to scan the entire beam without vignetting.

$$x \geq -\frac{(d+s)}{2} + \frac{1}{2}\sqrt{(d+s)^2 - 4(dt - et + es)}$$

Equation 10. Maximum half scan length with no vignetting at telescope objective lens.

Similarly, the sensor half width *g* must always be greater than *e* in order to not be limited by the sensor field of view.

3. RESULTS

To demonstrate the utility of the scanning pentaprism apparatus for a variety of use cases, we built a portable instrument based on the design parameters in Table 2. The instrument weighs 16.9 kg and the enclosure is a 650x152x200 mm rectangular volume, an architecture which is capable of being lifted by a single person into place for in situ measurements. The aperture on the scanning pentaprism is interchangeable for setting the aperture size and shape to one which optimizes pupil sampling, signal level, and image quality.

Parameter	**Symbol**	**Design Value**
Alignment telescope objective lens focal length	*f*	350 mm
Nominal pentaprism aperture spacing from lens	*s*	655 mm
Range of pentaprism travel	$\|2x\|$	350 mm
Objective lens clear aperture	*2e*	48 mm
Image sensor width	*2g*	8.4456 mm
Image sensor pixel pitch	N/A	3.45 μm

Table 2. Design parameters for demonstrator scanning pentaprism instrument.

The telescope focal length varies from the nominal value in Table 2 due to manufacturing tolerances, making it important to measure the as-built focal length to minimize systematic error. Additionally, the focal length varies with wavelength, and so characterizing it at various wavelengths allows the user to apply a focal length value that is appropriate for the beam being measured.

We measured the telescope focal length using an Optikos OpTest MTF bench. The bench collimates a multispectral point source generator with a reflective collimator to present an infinite object to the lens. The lens is mounted on a rotary stage which is used to induce small field angles by rotating the lens in the collimated beam. The angular encoder has 0.1 millidegree resolution and accuracy <0.3 millidegrees. The image location in the lens focal plane is tracked using an image analyzer on a three-axis translation stage with 0.05µm encoder resolution and accuracy <6µm. The rotary stage induced ±1 degree field angles while the off-axis translation of the image was tracked to measure the effective focal length as the ratio of the image translation to the corresponding field angles. Using this method, the focal length at 532nm was measured to be 349.648 ± 0.031 mm.

From this focal plane, the axial change in focus at eight additional wavelengths was measured by changing the bandpass filter in the multispectral object generator. The peak of the modulation transfer function (MTF) was used to determine best focus position at each wavelength. This process produced the chromatic focal length measurements in Figure 5.

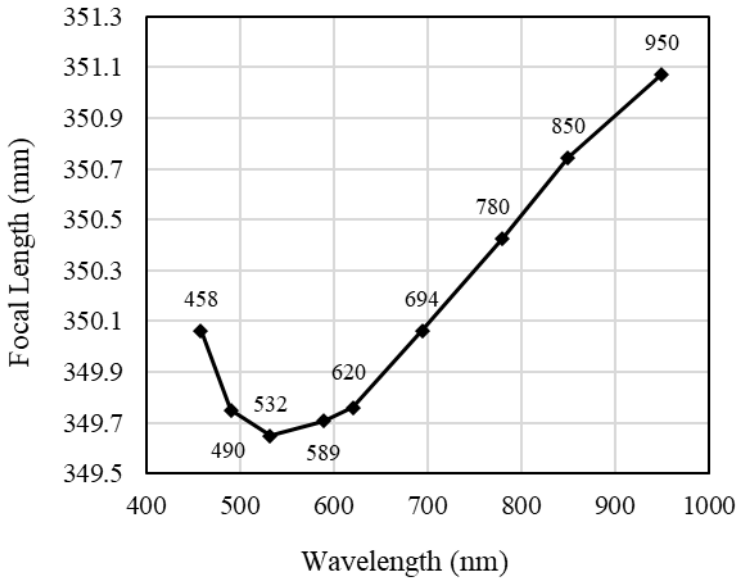

Figure 5. Chromatic focal length measurements of the alignment telescope objective lens used in the scanning pentaprism demonstrator.

Large Reflective Collimator

Minimum detectable departure from collimation due to defocus is fundamentally linked with the diameter of the beam. This relationship arises from the nature of the scanning pentaprism apparatus as a wavefront slope measurement, detecting angle of incidence (θ) rather than optical path difference (Φ) directly, according to the relationships shown in Figure 6. As the required scan length ($|2x|$) increases with the beam diameter, a given amount of optical path difference corresponds with lower slope error. This places tighter restrictions on the pointing stability of the alignment telescope. Rotations of the pentaprism can also introduce error from higher order deflection effects. This makes the measurement of large aperture collimators a challenging application.

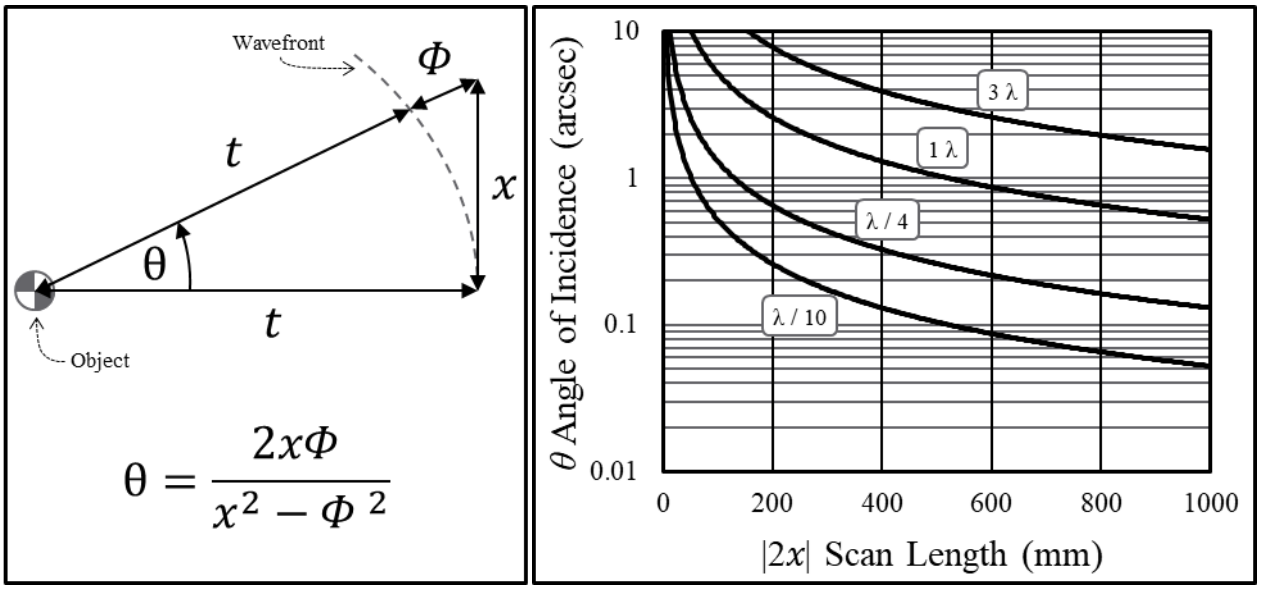

Figure 6. The relationship between wavefront error due to defocus and the change in angle of incidence that must be resolved by the scanning pentaprism to detect the defocus. Larger beams (represented by longer scan lengths) require higher sensitivity to angle of incidence changes.

For a large test case, we collimated the point source output of a 633nm laser unequal path length interferometer (LUPI) with a 405mm clear aperture, 3.048m focal length off-axis paraboloidal (OAP) mirror. A 450mm flat mirror retroreflected the collimated beam back into the OAP for interferometric feedback in the LUPI. Enough bench space was left in front of the flat mirror for the scanning pentaprism demonstrator, so that we could conveniently switch between confirming degree of collimation with the LUPI and measuring with the scanning pentaprism by moving the latter on and off of its riser mount.

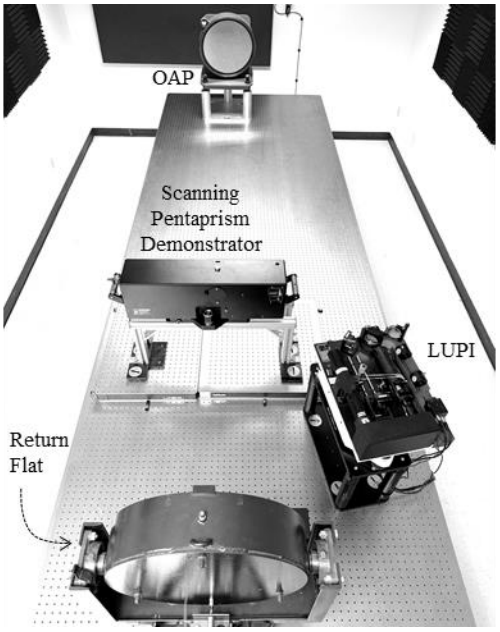

Figure 7. Setup photo for scanning pentaprism measurement of a large reflective collimator.

In this setup, the scanning pentaprism length of travel limited our maximum measurable beam size, and so the clear aperture measured by the LUPI was limited to this diameter for direct comparison of the Zernike power term reported by the LUPI and the total wavefront slope error detected by the scanning pentaprism. For the scanning aperture, a 2.5x17mm vertical slit was used. The centroid of the diffraction-limited image spot was calculated via a "center of mass" numerical integration of pixel intensities and their corresponding addresses. During data acquisition, images were taken at 60 scan positions uniformly distributed across the clear aperture, with five centroid measurements averaged at each scan position. The total measurement time for one scan was approximately 3.5 minutes. Ten scans were acquired, and the mean and standard deviation of each centroid value across the ten scans is shown in Figure 8. In addition to acquiring data at optimal collimation (Φ = 0.05 λ), the focus of the LUPI was adjusted to induce divergence for demonstrating detection of small departures from collimation (Φ = 1.48 λ and Φ = 2.33 λ).

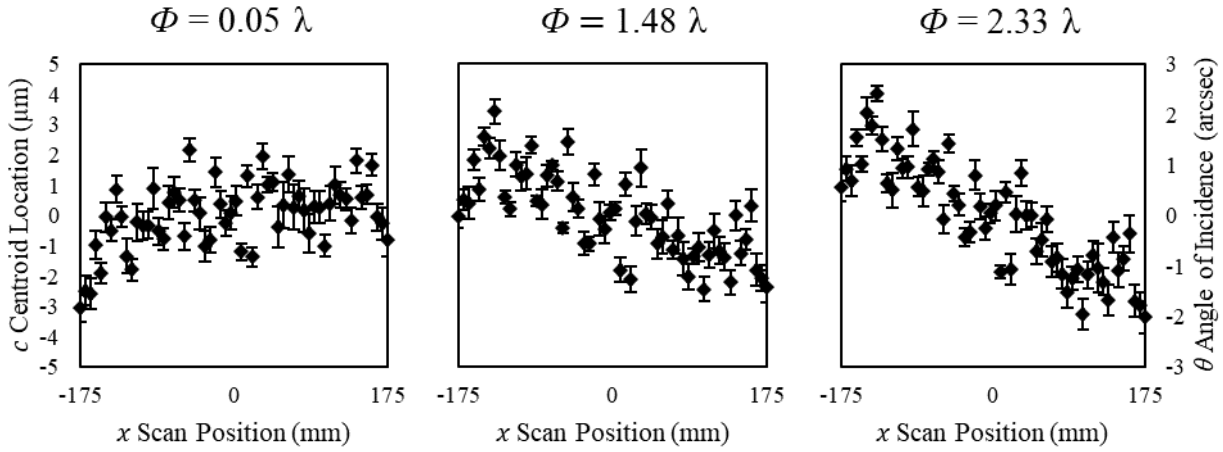

Figure 8. Ray fans of a 633nm point source collimated by an off-axis paraboloidal mirror into a 350mm beam. Data for three focus positions are shown with the Zernike power term reported by an independent interferometric measurement above each dataset for reference.

Refractive Collimator

We measured a Nikon 6D darkfield autocollimator as an example of a refractive collimator with low order aberrations. The centroid of the brightline crosshair was computed by fitting lines to the vertical and horizontal components of the crosshair and calculating their point of intersection. During data acquisition, images were taken through a 5x5mm square scanning aperture at 17 scan positions evenly distributed across the clear aperture. At each position, 10 centroid measurements were averaged to result in the data points shown in Figure 10.

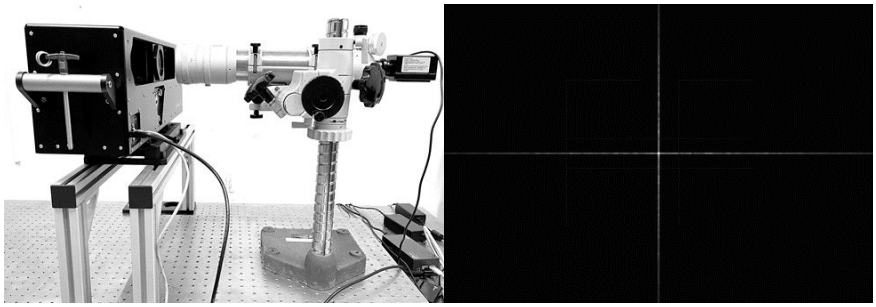

Figure 9. Setup photograph and crosshair image from scanning pentaprism measurements of a Nikon 6D Autocollimator.

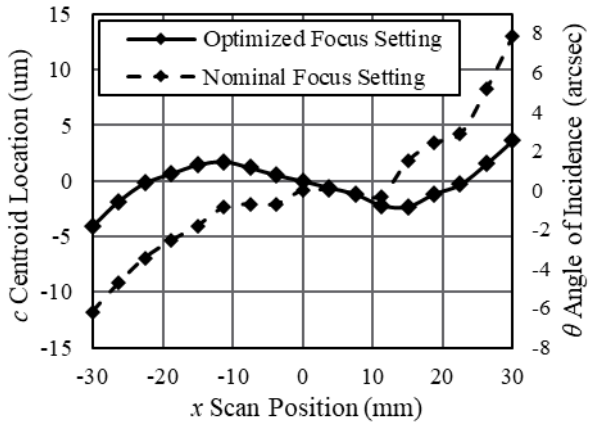

Figure 10. Ray fan data for the Nikon 6D Autocollimator. The nominal focus setting suggested by the manufacturer is shown, along with an optimized setting found using real-time feedback from the scanning pentaprism demonstrator to minimize collimation departure across the full pupil.

The cubic form of the ray fan indicates collimation is limited by third order spherical aberration. The Nominal Focus Setting is the collimation state when the focus adjustment ring on the autocollimator is set to its nominal "100" setting. The Optimized Focus Setting is a compromise position ("99.9" on the adjustment ring gradations) that minimizes departure from collimation across the 60mm pupil, which was found using the scanning pentaprism demonstrator for real-time feedback.

Finite Conjugate

To exercise more dynamic range, we measured a white light point source at various distances ranging from 1 to 26 meters. For distances less than 15 meters, the image traversed the entire sensor field of view, with the scan length limited to the range in which the entire image remained within the sensor active area.

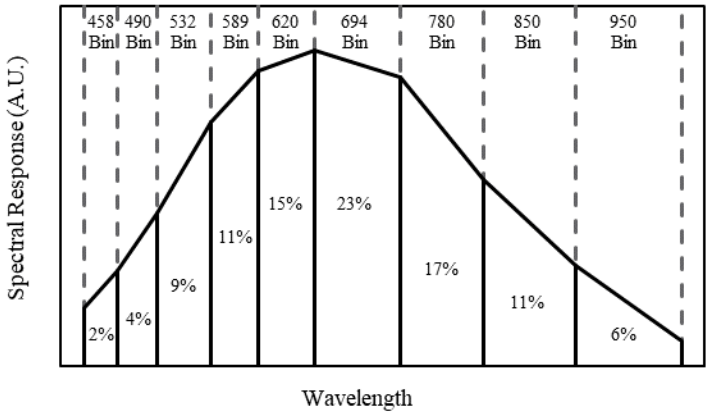

Figure 11. Spectral response of finite conjugate measurement comprising the point source emission spectrum, transmission of scanning pentaprism demonstrator optics, and sensor responsivity. The weights defined by the area under the curve within each bin were used to compute a weighted average focal length from the measurements in Figure 5.

Figure 11 is a weighting function defined by the spectral response of the measurement, which is calculated by multiplying the source emission spectrum, the spectral transmission of the scanning pentaprism demonstrator optics, and the spectral response of the image sensor. The function is divided into bins between the wavelengths at which the telescope focal length was measured in Figure 5. A weighted average of measured focal lengths from Figure 5 was calculated using the area under the curve within each corresponding bin of Figure 11 as weights, resulting in a polychromatic focal length of 350.127mm.

As an independent determination of object distance, we used a calibrated tape measure manufactured by The L.S. Starrett Company (Catalog number 530-30CM). The certified accuracy states that the total length error is no more than 0.100 inches over 100 inches.

Figure 12 shows the percent difference between measurements of object distance from the scanning pentaprism demonstrator and the calibrated tape measure. Most values are in the -0.2% to -0.4% difference range, with the 1 meter measurement being the only outlier at -2.1% difference. For reference, a line indicating the scan length used for each measurement due to sensor field of view is included.

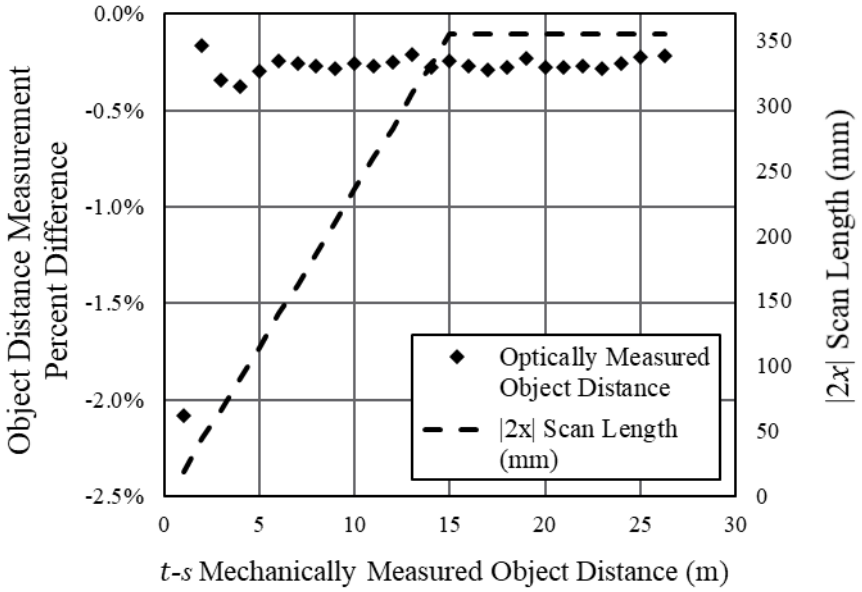

Figure 12. Comparison of object distance measurements of a white light point source using the scanning pentaprism demonstrator ("optically measured") and a calibrated tape measure ("mechanically measured"). For distances under 15 meters, the measurable beam size was limited by the field of view of the image sensor. The scan length dashed line shows the achieved scan length for each object distance.

4. DISCUSSION AND CONCLUSION

The scanning pentaprism technique has been utilized in testing large objective lenses and mirrors for over a century. In most of these cases, the pentaprism test investigates fabrication errors in the objective itself. Another application explored in this work employs the pentaprism in a passive rangefinder configuration, with the intent of measuring the projected object distance of a beam source. Because the digital alignment telescope used in combination with the pentaprism resolves an image of the object, software algorithms can accommodate a wide range of object geometries. The beam may also have any optical spectrum within the responsivity range of the image sensor. This versatility makes the scanning pentaprism test especially valuable where interferometry and Shack-Hartmann wavefront sensing are not possible, for beams large and small.

In this work, we demonstrated three object distance measurement scenarios: A large 633nm collimated beam showing sensitivity to residual power on the order of a wavelength, a green collimated beam exhibiting spherical aberration that

could be compensated with focus, and a white light point source at finite distances showing less than 0.4% difference from a calibrated tape measure in the 2 to 26 meter range. In addition to the distance and spectrum versatility that these examples show, there is potential for accommodation of complex object types. In particular, eyepiece reticles with graduations and other fine details may be measured with sufficiently uniform background illumination, opening up the application space into telescopic sights. The geometrical analysis in Section 2 informs design choices to be made when developing a system for measuring in any scenario.

5. ACKNOWLEDGMENTS

The scanning pentaprism demonstrator was designed and built by Lucas Delbanco. The adjustable kinematic base mount for alignment was designed and built by Michael Halligan. Dr. Jian Zhang provided the software for automating image acquisition, motion control, and centroid computation.

The authors would like to thank Dr. Stephen D. Fantone, whose organization, Optikos Corporation, funded this work.

REFERENCES

[1] Wetthauer and Brodhun, "Objektiv Untersuchungen," *Zeitschrift für Instrumentenkunde*, vol. 40, no. 5, pp. 96-97 (May 1920)

[2] R. N. Wilson, ""Matching Error" (Spherical Aberration) in the Hubble Space Telescope (HST): Some Technical Comments," *The Messenger*, no. 61, pp. 22-24 (1990)

[3] W. Scott Smith "Testing the 8.3-meter telescope optics", Proc. SPIE 2576, International Conference on Optical Fabrication and Testing, pp. 220-231 (August 1995); https://doi.org/10.1117/12.215597

[4] P. Su, J. H. Burge, B. Cuerden, J. Sasian and H. M. Martin, "Scanning pentaprism measurements of off-axis aspherics," Proc. SPIE 7018, Advanced Optical and Mechanical Technologies in Telescopes and Instrumentation, 70183T (25 July 2008); https://doi.org/10.1117/12.789588

[5] S. Qian, W. Jark, P. Z. Takacs, K. J. Randall and W. Yun, "In situ surface profiler for high heat load mirror measurement," *Optical Engineering* 34(2), pp. 396-402 (1 February 1995); https://doi.org/10.1117/12.194834

[6] S. Qian, W. Jark and P. Z. Takacs, "The penta-prism LTP: A long-trace-profiler with stationary optical head and moving penta prism," *Review of Scientific Instruments*, vol. 66, p. 2562–2569 (1995); https://doi.org/10.1063/1.1145658

[7] K. von Bieren, "Pencil beam interferometer for aspherical optical surfaces," Proc. SPIE 0343 Laser Diagnostics, pp. 101-108 (19 November 1982); https://doi.org/10.1117/12.933743

[8] P. C. V. Mallik, C. Zhao and J. H. Burge, "Measurement of a 2-meter flat using a pentaprism scanning system," *Optical Engineering* 46(2), 023602 (1 February 2007); https://doi.org/10.1117/1.2700386

[9] *Optics and optical instruments — Accuracy of optical transfer function (OTF) measurement*, ISO 11421:1997(E), Geneva, Switzerland, (September 15 1997)

[10] K. Mohammadi, Y. S. Lee and T. Jennewein, "Characterization of optical aberrations with scanning pentaprism for large collimators," CLEO: Applications and Technology, Imaging Techniques Across Multiple Modalities and Dimensions (ATh1D), San Jose, 2022.